Magnetotransport fluctuations in regular semiconductor ballistic quantum dots

R. Akis and D. K. Ferry
Center for Solid State Electronics Research, Center for Systems Science and Engineering, Arizona State University, Tempe, Arizona 85287
and Department of Electrical Engineering, Arizona State University, Tempe, Arizona 85287

J. P. Bird
Frontier Research Program, RIKEN, 2-1 Hirosawa, Wako, Saitama 351-01, Japan
(Received 13 June 1996; revised manuscript received 16 September 1996)

We present studies of the quantum-mechanical transport and the classical billiard transport through ballistic semiconductor quantum dots, where the transport is nonergodic or ''regular.'' These are shown to have quite similar behavior if the classical motion is limited to a collimated set of trajectories. These results are shown to agree substantially with experiments performed on actual semiconductor quantum dots. The results suggest that transport in regular semiconductor quantum dots is clearly distinguished from the equivalent transport in ergodic dots. In particular, the fluctuation spectrum is not random, but highly oscillatory and correlated. The correlation functions for these fluctuations show regular and periodic oscillations that contain only a few, often harmonically related, frequencies. This is fully in keeping with the expectations of semiclassical descriptions of the fluctuations in the density of states of such structures. [S0163-1829(96)03348-6]

I. INTRODUCTION

Reproducible fluctuations are a well-known quantum-mechanical correction to the conductance in disordered semiconductors.[1] Recently, there have also been observations of conductance fluctuations in small semiconductor *quantum dots*, in which the transport through the dot is ballistic in nature.[2–12] By ballistic we mean that the geometrical size of the dot is smaller than the elastic mean free path of the carriers. This has been made possible by advances in the use of electron-beam lithography and molecular-beam epitaxy.[13] In such structures, large-angle scattering of electrons occurs only at the dot boundaries. Experimental studies of such devices have shown the presence of both weak localization and conductance fluctuations, qualitatively similar to that observed in disordered systems. Generally it is believed that the fluctuations arise from interference between the complex ballistic paths in a manner analogous to impurity scattering in a disordered medium. In this ballistic case, the complexity is introduced by the reflections off of the dot geometry. However, there is evidence to suggest that weak localization occurs primarily due to interference between incoming particles and backscattered electrons at the entrance point contact.[5,14]

It is clear that the shape of the quantum dot strongly affects the details of the transport through it. Structures whose classical behavior is regular (integrable), such as the square, exhibit a weak localization signature that is characterized by a linear decay of the excess resistance with magnetic field. Contrastingly, structures whose classical behavior is chaotic (the stadium, for example) exhibit a Lorentzian line shape for the weak localization.[2–4,6,11,15–18] We note, however, that in open billiard systems, the presence of the leads also can induce phase-space filling behavior in quantum dots whose classical motion is otherwise integrable.[19] A transition between chaotic and regular behavior also has been seen in the weak localization line shape[11] in square quantum dots. The opposite transition in a stadium billiard in a magnetic field has been predicted.[20]

Conductance fluctuations in a chaotic quantum dot are characterized by their correlation function, which has a characteristic Lorentzian shape. This arises from the assumption that the ensemble of semiclassical trajectories through the quantum dot sweep out a wide range of ''areas'' (these areas are related to the enclosed flux winding number of the orbit). This is characterized by an exponential distribution as[15–18]

$$P(A)\sim e^{-\alpha|A|}, \tag{1}$$

where α is the inverse of the ''average'' area enclosing the flux. The correlation function of the conductance is related to this through

$$F(\Delta B)=\langle \delta G(B+\Delta B)\,\delta G(B)\rangle \propto \left| \int_{-\infty}^{\infty} dA\ \ e^{2\pi i \Delta B A/\phi_0} P(A) \right|^2$$

$$\propto \left[1+\left(\frac{2\pi \Delta B}{\alpha \phi_0} \right)^2 \right]^{-2}, \tag{2}$$

where $\phi_0 = h/e$ is the quantum of flux.

Recently, however, there have been measurements of conductance fluctuations in square dots[21,22] that do not appear to be irregular but are quite periodic, and their correlation function is characterized by large-amplitude oscillations. A Fourier spectrum of these correlation functions exhibits families of harmonically related peaks; sometimes only one family appears, while at other times multiple families appear. These results cannot be explained by the above theory, nor by an ensemble of trajectories that includes *all* possible classical paths through the dot. Rather, the excitation of the regular behavior is thought to proceed through the collimation effects of the quantum point contact. In the classical limit, in which a great many waveguide modes are passed by the

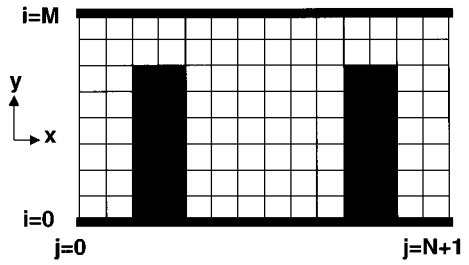

FIG. 1. Geometry of the quantum dot and quantum point contacts that are considered in this study. The grid represents the underlying mesh on which the calculations are performed, though, in practice, the mesh is much finer.

point contact, the particles form a beam centered on the transport axis of the contact.[23] However, when only a few modes are passed, the quantization of the transverse momentum can cause a diffraction effect that leads to the beam exiting the point contact at a significant angle away from the transport axis.[24] This axis is defined by the line connecting the two aligned leads shown in Fig. 1 below. Hence excitation of the quantum dot proceeds via a collimated beam oriented away from the axis, which then can excite a set of regular orbits within the dot.

In this paper, we examine the transport through such regular quantum dots, both by a careful study of the quantum transport obtained by a direct solution of the Schrödinger equation and by the study of a selected set of classical billiard trajectories within the dot. We show that the classical trajectories have a strong connection to scarring of the quantum wave function,[25] and the computed correlation functions and Fourier spectra are shown to exhibit a close connection to those measured experimentally. In the next section, the transport obtained from the Schrödinger equation is discussed, while the classical billiard approach is described in Sec. III. We then turn, in Sec. IV, to a comparison with the experiments. Finally we summarize the results in Sec. V.

II. QUANTUM BEHAVIOR OF THE REGULAR DOT

As displayed in Fig. 1, the general situation is one in which ideal quantum wires, which extend outward to $\pm\infty$, are connected to the quantum dot. This quantum-mechanical problem can be solved by using an iterative matrix method[26] applied to the discretized version of the Schrödinger equation, obtained by keeping terms up to first order in the approximation of the derivative:

$$(E_F-\mathbf{H}_j)\psi_j+\mathbf{H}_{j,j-1}\psi_{j-1}+\mathbf{H}_{j,j+1}\psi_{j+1}=0, \qquad (3)$$

where ψ_j is a M-dimensional vector containing the amplitudes of the jth slice. The problem is solved on a square lattice of lattice constant a with the wires extending M lattice sites across in the x direction and the region of interest being broken down into a series of slices along the y direction. In this equation, the $\mathbf{H}_j$ matrices represent Hamiltonians for individual slices and the matrices $\mathbf{H}_{j,j-1}$ and $\mathbf{H}_{j,j+1}$ give the interslice coupling. By approximating the derivative, the kinetic-energy terms of Schrödinger's equation get mapped onto a tight-binding model with $t=-\hbar^2/2m^*a^2$ representing nearest-neighbor hopping. The potential simply adds to the on-site energies. This equation can be used to derive a transfer matrix that allows us to translate across the system and thus calculate the transmission coefficients that enter the Landauer-Buttiker formula to give the conductance. Transfer matrices, however, notoriously are unstable due to the exponentially growing and decaying contributions of evanescent modes. This difficulty can be overcome by performing some clever matrix manipulations and calculating the transmission by an iterative procedure rather than just multiplying transfer matrices together. The full details of this technique are given in Ref. 26. This method, in some ways, is quite similar to the recursive Green's-function techniques[27,28] that typically are used to solve these problems, and a comparison has shown good agreement between the two methods. The amplitudes

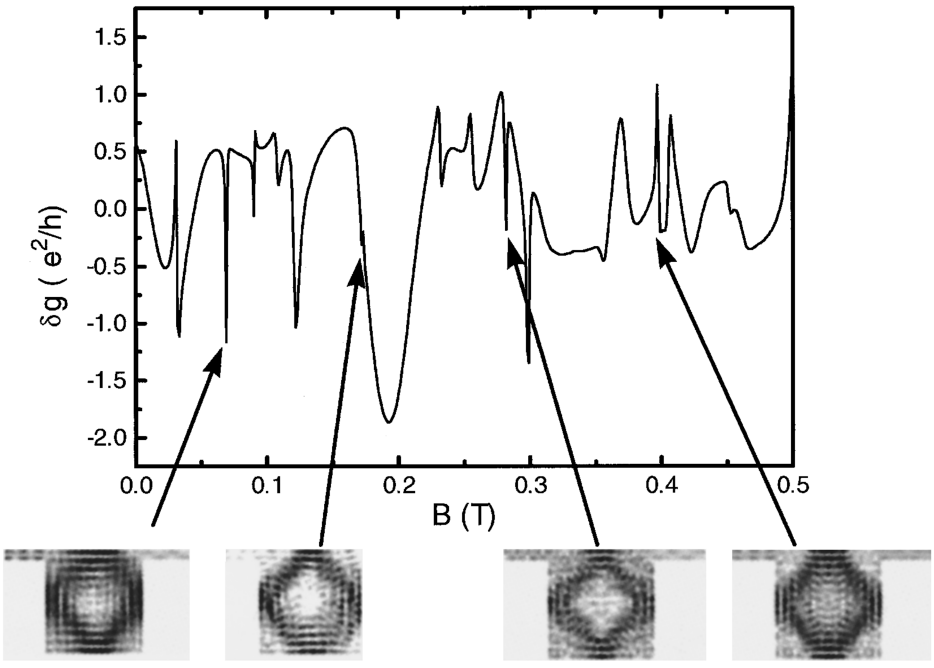

FIG. 2. Conductance fluctuations vs magnetic field for the 0.3-μm dot discussed in the text. Four resonance features that appear in the curve are also indicated and $|\psi(x,y)|$ vs x and y in the quantum dot is plotted for each of these features. Darker shading corresponds to higher amplitude.

of the wave functions at specific values of x and y can be found easily by backward substitution after the iteration is performed.

The quantum dots we study are nominally square in shape. They are connected to two leads, which provide the input and exit ports, as shown in Fig. 1. The leads are usually taken at the top of the dot, as illustrated, but a staggered positioning of the leads will also be discussed briefly. Although the ports are normally aligned, straight through trajectories are not a problem due to the diffraction effects of the quantum point contacts themselves, as discussed above (we will return to this point below). A magnetic field is applied normal to the plane of the dot and the carrier density is typically taken to be 4×10^{11} cm^{-2} in order to compare with the experiments of Refs. 11 and 21.

We first present an illustrative example of our calculations. In Fig. 2, conductance fluctuations as a function of magnetic field are plotted for a 0.3-μm square dot with 0.04-μm port openings, which allow two modes to enter and exit the dot. Instead of a random aperiodic variation with magnetic field, a series of nearly periodic oscillations is evident. Also apparent are several resonance features. In particular, we point out a set of resonances at $B\sim0.069$, 0.173, 0.283, and 0.397 T (while the feature is difficult to see at $B=0.173$ T, it appears as a small notch in the curve). These are marked with arrows. Note here that these features occur with virtually periodic spacing. The wave functions corresponding to these four resonances are also displayed at the bottom of the figure. What is shown in each case is $|\psi(x,y)|$, with the darker shading corresponding to higher wave-function amplitude. Strikingly, essentially the same diamond-shaped pattern occurs in each case. This pattern is highly reminiscent of the ''*scars*'' that have been observed in calculations performed for stadium-shaped quantum structures,[29] in that the quantum-mechanical amplitude appears to follow a single underlying classical orbit. Given that the period for the reappearance of the diamond is $\Delta B\sim0.11$ T and using the criterion familiar from the Aharonov-Bohm effect, that $\Delta\phi/\phi_0=2\pi$ for the difference in magnetic flux, one obtains $A\sim0.04$ μm^2 for the enclosed area, which corresponds well to the enclosed area of the diamond.

In Fig. 3, we show the conductance fluctuations for several other examples of a 0.3-μm quantum dot. In the figure, conductance fluctuations as a function of the magnetic field are shown for (a) 0.09-μm port openings; (b) 0.04-μm port openings, but with the entry port at the top of the dot and the exit port at the bottom to minimize the possibility that electrons might take direct paths through the dot; and (c) 0.04-μm port openings, but with circularly rounded corners and openings. As above, the 0.04-μm port openings support two propagating modes, while the 0.09-μm port openings allow four. Once again, in each case a series of nearly periodic oscillations is evident. Also apparent are sets of resonance features. In fact, many of these resonances appear in approximately the same location in all three panels, as well as corresponding closely with the initial example displayed above. In particular, the set of resonances at $B\sim0.069$, 0.173, 0.283, and 0.397 T are apparent in these three examples as well. As one may expect, the curve for the wider port case [Fig. 3(a)], in which two more modes are passing through the leads, is somewhat smoother, with only about half the resonance features as in Fig. 2. This is almost certainly a result of the effect of level broadening induced by the port opening. However, the basic periodicity of the oscillations is quite similar to the narrow port case above. For Fig. 3(c), the bottom corners of the dot are of the form of semicircles of radius 0.1 μm, while the entry ports are also rounded with radius 0.05 μm, though the narrowest width of the opening is the same as in the first example. It is evident that this rounding by itself does not destroy the resonance effects (in fact, some of the resonances are even stronger in this case), nor does it strongly affect the basic underlying periodicity. The same comments can be made about offsetting the port openings as shown in Fig. 3(b). From these results, we may surmise that the resonances and the fluctuations are both basic properties of the quantum dot itself. However, only those intrinsic properties that couple to the input and output leads can be expected to be reflected in the conductance.

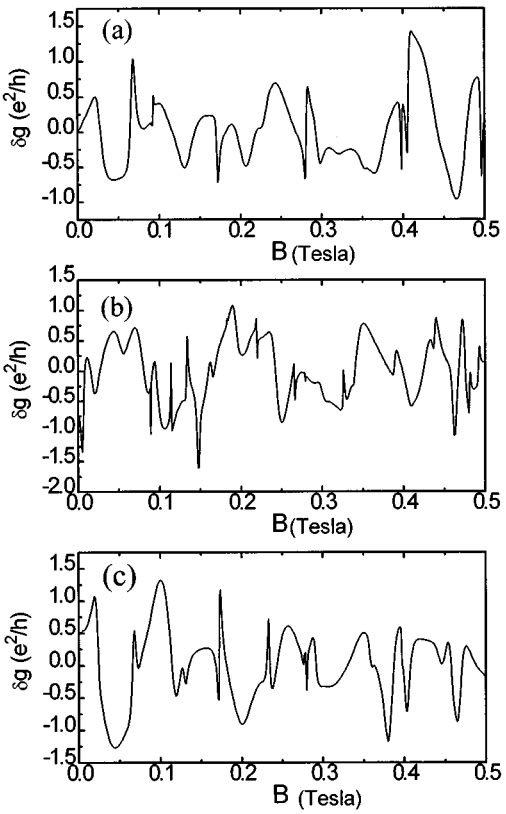

FIG. 3. Conductance fluctuations vs magnetic field for 0.3-μm quantum dots with (a) port openings that are 0.09 μm; (b) port openings that are 0.04 μm, but with staggered leads, (c) port openings that are 0.04 μm, but with the corners and openings of the dot not having been rounded.

In Fig. 4, we plot more examples of wave functions in quantum dots. The wave functions shown in Fig. 2 as pointed out earlier looks to be scarred by a periodic classical orbit. However, since the structure is ostensibly regular, the fact that there appears to be a correspondence to the classical picture should not be a surprise since the wave functions should be concentrated along the projections of the invariant tori of the regular trajectories in classical phase space. However, it is worth pointing out that this image *differs radically*

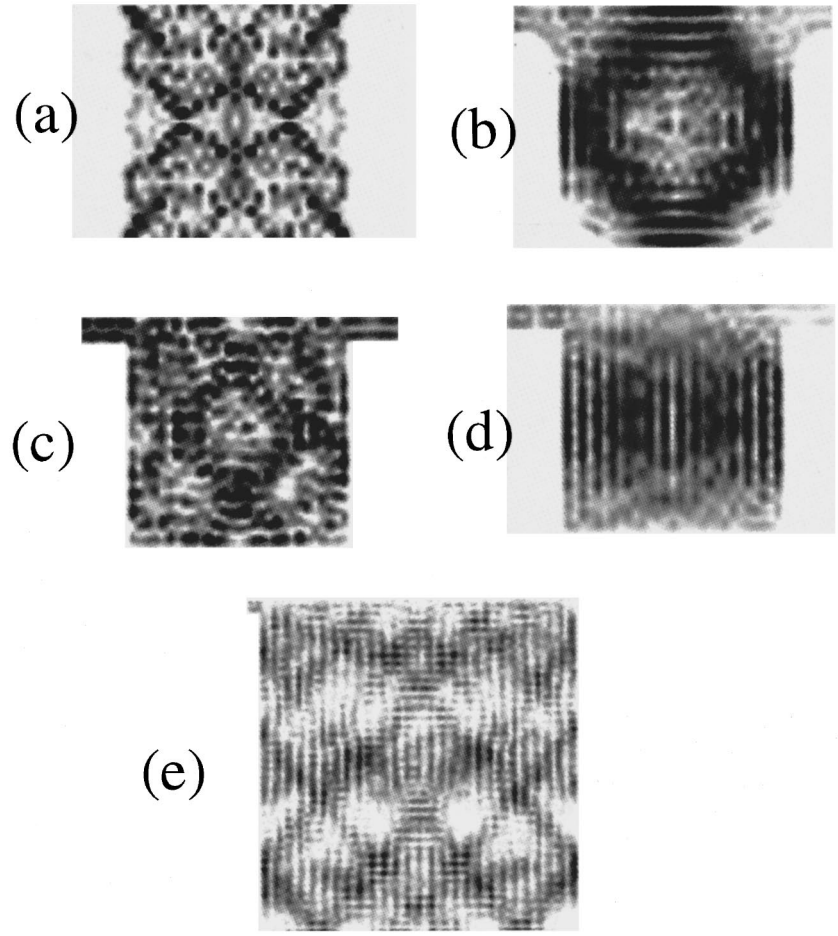

FIG. 4. $|\psi(x,y)|$ vs x and y is plotted. Darker shading corresponds to higher amplitude. The four pictures correspond to (a) a dot completely enclosed by tunneling barriers; (b) the rounded dot, with $B=0.282$ T; (c) the dot with 0.04-μm openings at $B=0.231$ T; (d) same as in (c), but with $B=0.299$ T; and (e) a 0.8-μm dot at $B=0.0056$ T.

from what occurs in a *closed* dot, in which the amplitude for an eigenstate is distributed much more uniformly and one *cannot* make an association with a single orbit. To emphasize this point, in Fig. 4(a), we plot $|\psi(x,y)|$ for a 0.3-μm dot formed by two tunneling barriers, with the barrier height equal to the Fermi energy of the previous example and a barrier width of 0.05 μm. The transmission as a function of B for this case consists of a series of very sharp tunneling peaks, so the dot is a very close approximation to a closed system. The wave function in this image corresponds to a resonant tunneling peak at $B=0.165$ T and is a fairly typical result. Comparing Fig. 4(a) with the wave functions displayed in Fig. 2, it is clear that the results are quite different when the electrons are made to enter the dot in a narrow beam by the contact, and what we see is consistent with a reduction in the classical phase space sampled by the electrons, in turn introduced by collimating action of the leads, as will be discussed in Sec. III. Once again, we conclude that the collimation by the quantum point contacts selects a set of properties (trajectories) of the quantum dot.

In Fig. 4(b), $|\psi(x,y)|$ is plotted for $B=0.282$ T, but in this case for the rounded dot example discussed in the context of Fig. 3. We see that rounding does not prevent the diamond scar from forming. This result is reassuring, since one does not expect the experimental dots to be perfectly square in shape.

In Fig. 4(c), $|\psi(x,y)|$ is plotted for the 0.3-μm dot with the 0.04-μm port opening, except now we have set $B=0.231$ T, which corresponds to another resonance feature in Fig. 2. Here we see another scarlike feature, but in this case it has the appearance of two intersecting rectangular orbits. In comparison to the diamond-shaped scar, this feature is somewhat less well resolved. Making an estimate of the enclosed area of one of the rectangles, we get $A\sim 0.04$ μm^2, approximately the same as the diamond. Given this, we should also expect to see the double rectangle at $B\sim 0.11$–0.12 T; however, we cannot make out this evidently more delicate feature, though there is a resonance in the conductance fluctuations in about the right location. However, it is worth noting that the resonance at this field is somewhat less sharp than the one at $B=0.231$ T. The double rectangle also occurs for the offset port and rounded dot cases at $B=0.231$ T, while it does not appear in the dot with the wide opening, which shows no resonance at this value of B. Not surprisingly, for B fields falling in between the resonances, the wave function in general is much less organized. As mentioned above, a resonance does not necessarily yield a well-defined scarlike feature, though this seems to be related to the sharpness of the resonance. It should also be noted that some of the resonances that occur in Fig. 2 yield wave functions that are quite similar to the ''bouncing ball'' plots familiar from the stadium billiard problem.[26] An example of this is shown in Fig. 4(d), which was generated with the 0.04-μm port opening, but with $B=0.299$ T. Another such feature occurs at $B=0.1$ T, but in that case the orientation of the bouncing ball is vertical rather than horizontal as it is here.

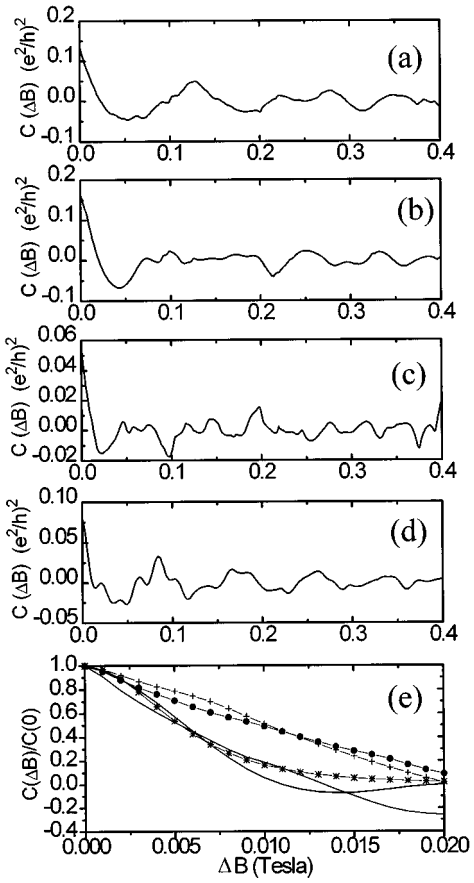

FIG. 5. Correlation function $C(\Delta B)$ vs ΔB plotted for the four cases considered in (a) Fig. 2(b)–2(d) and Figs. 3(a)–3(c). In (e), the normalized correlation function $C(\Delta B)/C(0)$ is plotted for low fields for the above cases with circles corresponding to (a), crosses to (b), a dashed line to (c), and a solid line to (d). A fit to case (d) using Eq. (2) is also plotted (stars).

So far, we have concentrated our discussion on 0.3-μm dots. We have also seen the diamond-shaped pattern in both smaller (0.2-μm) and larger (0.8-μm) dots for the same electron density. Many more complicated patterns are also evident in the larger dot. An example is shown in Fig. 4(e), which occurs for the 0.8-μm dot with $B=0.0056$ T. The leads here support three modes. Needless to say, the Aharonov-Bohm analysis performed for the 0.3-μm dot is no longer a simple matter here, and the results, at least in terms of the scarring, become somewhat more difficult to interpret.

In Figs. 5(a)–5(d), we plot the correlation functions $C(\Delta B)$ obtained from the conductance fluctuations displayed in Fig. 2 [Fig. 5(a)] and Fig. 3 [Figs. 5(b)–5(d)]. To eliminate any possible effects of a weak localization peak, they are calculated for a range between 0.1 and 0.5 T and we have used averaging to minimize any statistical errors. The correlation functions all show large negative excursions and oscillations. The oscillations appear to be quasiperiodic, a reflection of the periodicity apparent in the fluctuations themselves in Figs. 2 and 3. These oscillations are least prevalent in the case with the large openings, though they are still apparent in that case. Comparing Fig. 5(a) with Fig. 5(c), the offset port case, the former has large oscillations with much smaller ones superimposed on top of them, whereas the latter is dominated more by the smaller oscillations. Fig. 5(d), for the rounded dot, appears to fall in between Figs. 5(a) and 5(c). In Fig. 5(e), we consider the low-field behavior of correlation function, with the crosses, circles, dashed and solid lines corresponding to Figs. 5(a), 5(b), 5(c), and 5(d) from above, respectively. Unlike the previous panels, the correlation function has been normalized by $C(0)$ in each case. Here Figs. 5(a) and 5(b) display approximately the same correlation field B_c (the ΔB value that yields the half maximum value of $C(\Delta B)$], about 0.01 T. The correlation function for the offset port case drops more quickly tan in Fig. 5(a) or 5(b), with $B_c=0.007$ T, but still shows power-law behavior. For the rounded port case, the correlation function drops even more quickly ($B_c=0.005$ T) and the curve is significantly more rounded than the others, which is more in line with the prediction for chaotic systems given in Eq. (2). For comparison, we plot a fit using (2), represented by the diamond symbols. The fit yields an average enclosed area of $\alpha^{-1}=0.079\ \mu\mathrm{m}^2$, which is close to the entire area of the dot 0.09 $\mu\mathrm{m}^2$. That the rounded dot shows the best correspondence to (2) is not particularly surprising since the dot in this case has a geometry approaching that of a half stadium, which is known to be chaotic. We point out, however, that observation of a Lorentzian correlation function is not *a priori* evidence for chaotic behavior, and the above discussion indicates that the dot remains quite regular. This feature is confirmed by the classical calculations, which show that, for uniform injection of particles into a perfectly regular cavity, strong phase-space filling is obtained, in spite of the underlying regularity.

In Fig. 6, we plot the Fourier transforms of the correlation functions from Fig. 5. As with the classical examples to be seen below, these power spectra indicate that just a few discrete frequencies can dominate the behavior, and it is evident that many of these peaks are harmonically related. For example, the offset port in Fig. 6(c) has a group of peaks occurring at approximately 9, 16, and 24 T^{-1}, with the peaks at 13 and 26 T^{-1} constituting a second group. In fact, the peaks seem to occur in more or less the same positions in all four cases (in particular, the two groups of peaks mentioned above), though their relative weights are quite different in each example. It is noteworthy that prominent peaks occur in the region ~ 8–$9\ \mathrm{T}^{-1}$ for Figs. 6(a)–6(c) and, while less prominent, it also appears in Fig. 6(d) as well. As mentioned earlier, we repeatedly observed the diamond-shaped wave functions for all these examples. The spacing of these scar-like features yield values of $(\Delta B)^{-1}$ of $\sim 8.7\ \mathrm{T}^{-1}$, which corresponds fairly well with the positions of these peaks.

III. CLASSICAL BILLIARDS

Periodic orbits have played a large theoretical role in the computation of semiclassical quantization of bound states for many years, dating back to the Einstein-Brillouin-Keller view of quantization. The modern revival of work in this area apparently was begun by Gutzwiller,[30] who examined the relationship between the periodic orbits of a classical system and the corresponding solutions of the Schrödinger equation in the case where neither corresponded to a separable system. Balian and Bloch[31] and Berry and Tabor[32] began studies of the level densities and eigenvalues of nonin-

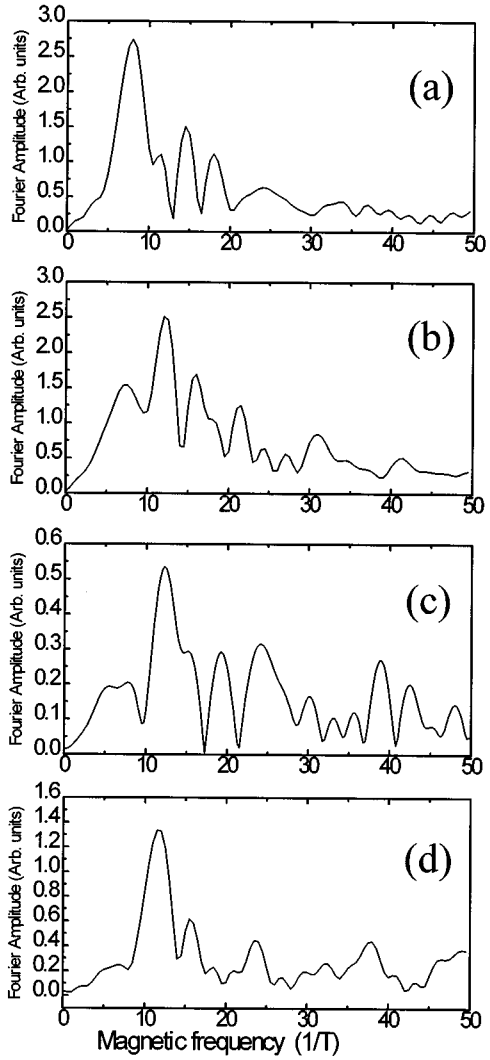

FIG. 6. Fourier transforms of the correlation functions displayed in Figs. 5(a)–5(d).

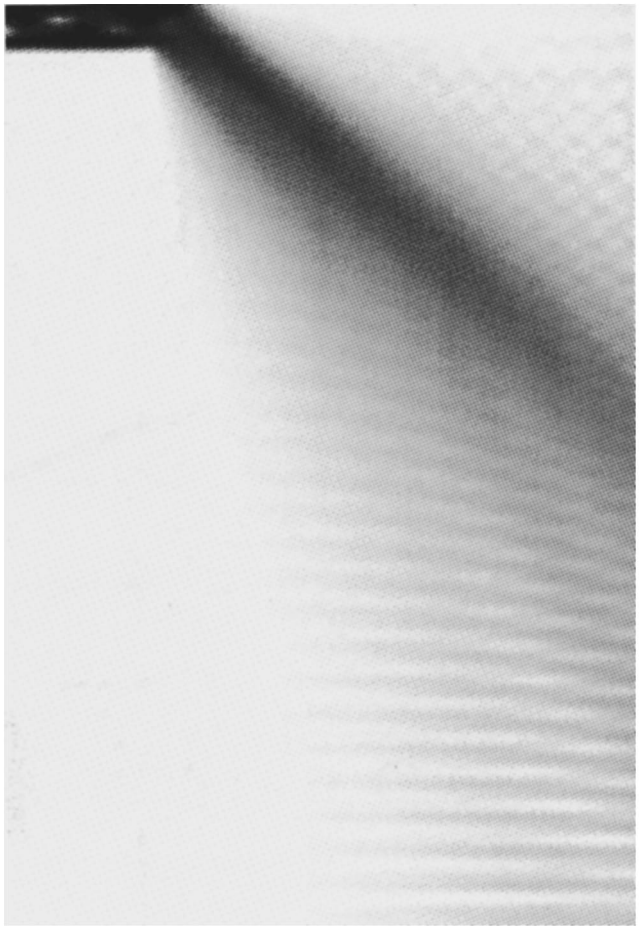

FIG. 7. Collimation of the beam is apparent in this picture, which describes the entry of particles from a point contact (0.05 μm wide) in which only two modes are allowed to propagate into a much wider quantum wire (0.8 μm wide).

tegrable systems. Perhaps the most important result, though, was the observation that certain (what were thought to be) unstable periodic orbits produced scars in the quantum wave functions.[29] More recent studies indicate that the ''imprints'' of these orbits persist up through thousands of states,[33] a result that suggests that the closed orbits are quite stable in regular systems and only become unstable as one passes to the ergodic regime, which seems to be replicated as one passes from the semiclassical to the quantum regime. Nevertheless, how is one to choose these semiclassical orbits? Traditionally, one examined all possible classical paths from the input to the output.[15,16] But, in such ballistic quantum dots, this produces essentially a phase-space filling and ergodic behavior of the transport, which agrees closely with chaotic dot studies.[15–18] There is a clear difference between the behavior obtained when al possible trajectories are investigated and when only a limited set of trajectories are investigated.[34] We focus solely on the case for a collimated beam of particles. The crucial assumption in doing this is that the quantum point contact imposes a boundary condition on the particles, in which the entry angle is determined by the wave mechanical nature of propagation through the quantum point contact. As discussed above, the quantum point contact effectively collimates the beam into a relatively narrow ray of particles, and we illustrate this collimation in Fig. 7 using the solution to the quantum-mechanical case described in Sec. II. Here we depict a narrow contact connected to a much wider quantum wire. What we are seeing here is the result of the waveguiding effects of the contact. With very few modes present in the leads (in this case 2), the entry angle of the electrons becomes strongly restricted by the *quantization* of the wave vectors in the y direction. It should be emphasized that this picture corresponds to the zero-field case. Thus the rotation of the electron beam away from the x axis cannot be attributed to the bending of the electron trajectories by the magnetic field. It is this collimation that is important for selecting or exciting the regular orbits of the particles, a point that is discussed further below.

In the first three panels of Fig. 8, we show Poincaré plots for entry angles of 74°, 59°, and 36° (the angles are not magic, but are chosen merely as fractions of $\pi/2$) from the y axis for the case of a magnetic field of 10 mT. Poincaré plots essentially are cross sections through part of the classical phase space. What appears on the plot are the intersection points of the classical trajectories with the cross-sectional surface. These plots give a good indication of

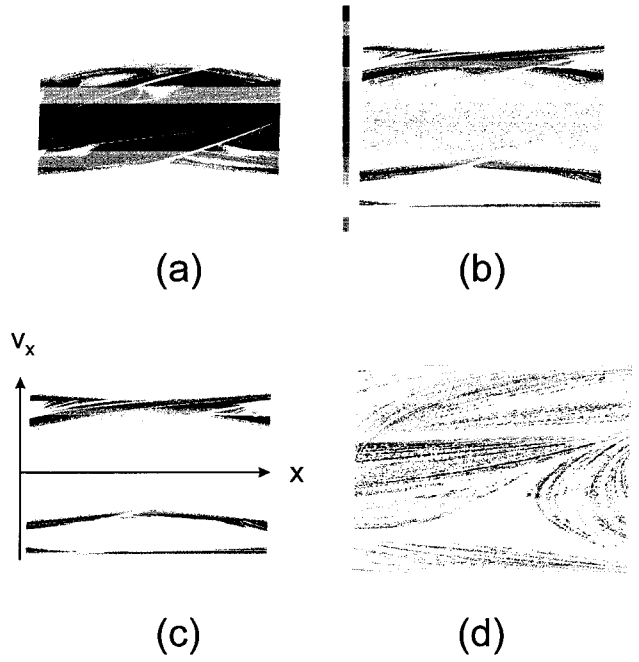

FIG. 8. Poincaré plots for a magnetic field of 10 mT and for entry angles of (a) 63°, (b) 56°, and (c) 36°. The vertical gray map in (b) is a calibration of the y velocity in the plots ranges from 0 up to 3×10^7 cm/s, and applies to the other three panels. Another Poincaré plot is shown in (d), in this case for a magnetic field of 50 mT and an entry angle of 54°. Note that the axes plotted in panel (c) also apply to the other three panels in the figure. The x range is 0–1.0 μm and the v_x range is from -3×10^7 to 3×10^7 cm/s.

which portions of the multidimensional phase space are visited. In the present case, the surface is taken as the bottom of the dot (particles pass through the surface just prior to reflection from the bottom boundary) and illustrates the x position and x velocity for particles that impinge on this surface (this general geometry is used throughout this paper).[35] The magnitude of the particle velocity has been set to 3×10^7 cm/s as this yields a kinetic energy equal to the Fermi energy used in the quantum calculations. The gray scale corresponds to the y-directed velocity and varies from 0 to 3×10^7 and is shown for convenience. The vertical scale for the x velocity ranges from -3×10^7 to 3×10^7. As the entry angle is reduced, the phase-space filling is greatly reduced and there appears to be a critical angle for which this occurs. This angle is related to the magnetic field, but the behavior of the ballistic transport is anything but ergodic. We can see this somewhat better in Fig. 8(d), where the Poincaré plot is shown for $\theta=54°$ and $B=50$ mT. Here, although only a small number of particles have been used so that the discrete trajectory maps are observable, it is clear that the magnetic field induces curvature in the ballistic orbits that causes an apparent phase-space filing through precession of the magnetic orbits, even though the motion is fully integrable. For further insight, we can actually compute the histogram for the Poincaré plot. That is, we plot a three-dimensional picture, whose z axis is the frequency at which any single (x,v_x) point is occupied in the Poincaré plot itself. In Fig. 9(a), we plot this for the apparent phase-space filling motion of Fig. 8(a). There are clear scars throughout the plot that are quite reminiscent of the trajectory maps of Figs. 8(b) and 8(c). However, the plot in Fig. 9(a) is the logarithm of the occurrence (9×10^6 particle trajectories were followed), so that there are orders of magnitude difference between the peaks on the residuals of the proper trajectories and the valleys around $v_x=0$. Finally, it should be remarked that the area distribution function [Fig. 9(b)] does not fit Eq. (1) at all; it is essentially one sided (only a positive area) and is not fully exponential in its dependence upon the area. The two peaks occur at zero area and an area corresponding roughly to an enclosed area of 0.48 μm^2 (this is for the 1.0-μm dot), which compares well with the scaling from the smaller dots for the prime frequencies of the periodic orbits. It is relatively clear that just having phase-space filling is not sufficient to say that the motion is ergodic. Quite the opposite, in these regular (square) quantum dots, the transport for a collimated input beam is completely regular, even with open leads and the presence of a magnetic field.

The magnetotransport through the dot can be computed by determining the transmission probability of electrons

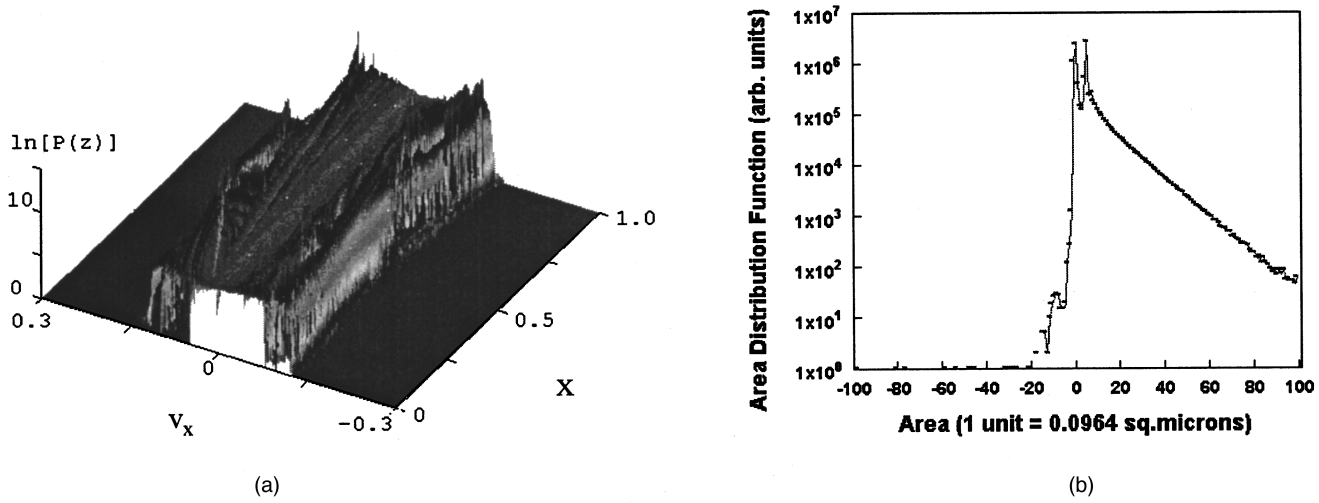

FIG. 9. (a) Poincaré histogram corresponding to Fig. 8(a). (b) Area distribution function for this case of regular transport.

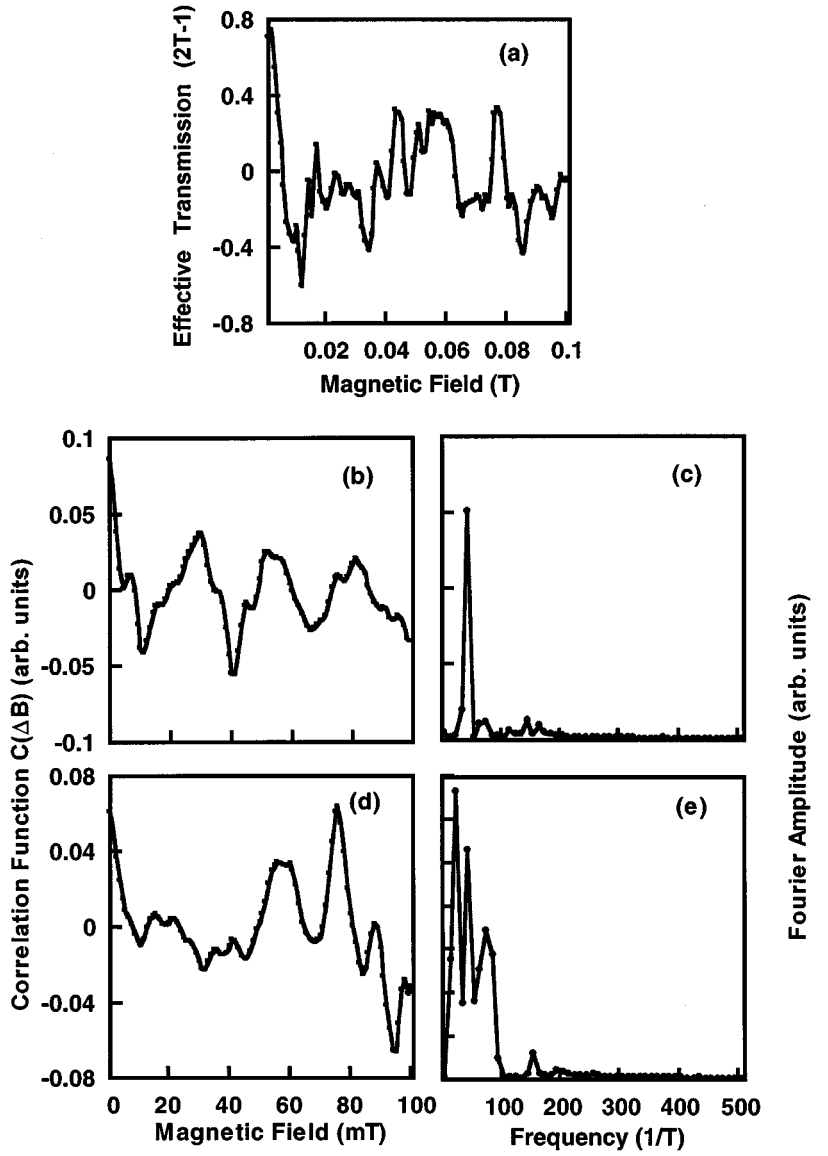

FIG. 10. Transmission probability plotted as $2T-1$, in order to remove a significant part of the magnetic-field-independent conductance, for a 1.0-μm quantum dot with an entry angle $\theta=63$. (b)–(e) correspond to the correlation function (left panels) and its Fourier transform (right panels) for two different entry angles into the 1.0-μm dot. The top row corresponds to $\theta=54$, while the bottom row corresponds to $\theta=63$.

through the dot.[36] In Fig. 10(a), we plot such a magnetoconductance trace for an entry angle of 63° for a 1.0-μm dot. The actual plot depicts $2T-1$ as this removes most of the background average conductance and highlights the fluctuations. It is clear that the fluctuations in this case have a significant tendency toward regular oscillatory properties and are not characterized by the random nature expected of ergodic behavior. We can see this better in the correlation function $C(\Delta B)$ of the conductance. This correlation function and its Fourier transform are shown for two different entry angles in Figs. 10(b) and 10(c). The correlation function described by Eq. (2), in terms of an exponential distribution of areas, is positive definite. This is anything but the case for these regular trajectories, and extensive negative excursions and oscillations are present in these correlation functions. Indeed, these now resemble the correlation functions obtained for the fully quantum case in Sec. II. Again, the Fourier transform illustrates that only a few discrete frequencies are present in the correlation function. These frequencies seem to be harmonically related (or compose very few families of harmonically related frequencies). Not all harmonics are always present, and we do not understand the relationships between the harmonic amplitudes at this time. Nevertheless, it is clear that this regular transport produces fluctuations that are the result of a few multiply recurring orbits within the quantum dot, a result that is inherent in the quasiclassical quantization of the dot itself.[31] Indeed, the underlying theory of such quasiclassical quantization suggests that the spectrum should be made up of contributions from families of harmonically related orbits,[32] a result in keeping with the Einstein-Brillouin-Keller theory of quantization.

IV. EXPERIMENT AND DISCUSSION

Now, as a summary of the theoretical discussion above, we compare it with experiments carried out in 0.3-μm dots fabricated in GaAs/$Al_xGa_{1-x}As$ heterostructures. Split-gate quantum dots were formed in a heterojunction wafer using standard lithographic techniques. After low-temperature illumination, the carrier density and mobility of the wafer were found to be 5.1×10^{11} cm^{-2} and 70 $m^2/V\,s$, respectively. The gates allowed definition of a

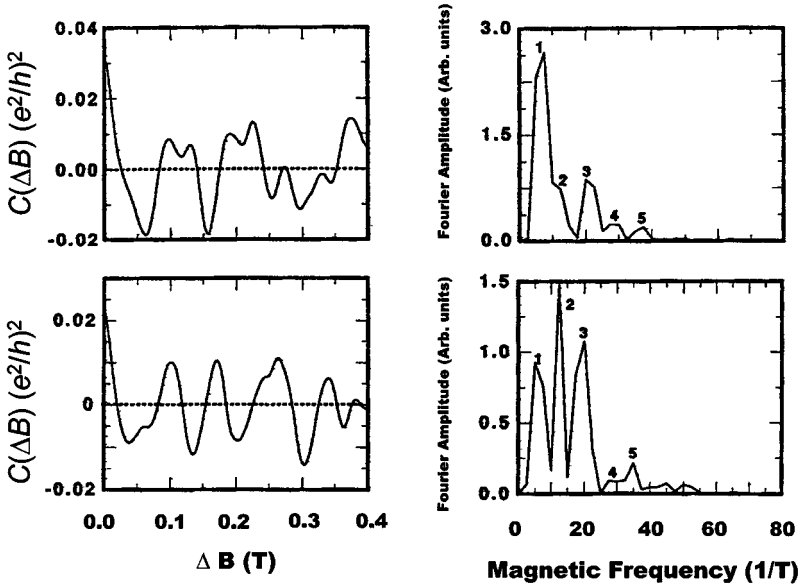

FIG. 11. Correlation function (left) and power spectra (right) of the fluctuations in the 0.4-μm (lithographically defined) quantum dot for two different gate voltages. The dot resistances are 10 and 26 kΩ for the top and bottom rows, respectively.

square cavity, with lithographic dimension of 0.4 μm. The well-defined Aharonov-Bohm oscillations at high magnetic field[37] enabled a determination of the actual dot size, after accounting for depletion around the gate edges, to be approximately 0.3 μm. In Fig. 11, correlation functions and the Fourier transforms of these correlation functions are shown for two different gate voltages. It is clear that there is a clear dominance of the transport by probably a single or a very few orbits. Such dominance is quite different from what is expected for ergodic transport, a conclusion that is confirmed by the observed fact that the correlation field B_c is independent of lead opening in the quantum point contacts and of the temperature (measurements were made at a base temperature of approximately 30 mK).[21] The insensitivity to lead opening width is also in agreement with our quantum simulations shown in Sec. II, which yielded almost the same value of B_c when the lead openings were increased from 0.04 to 0.09 μm, and shows that just a few *stable* orbits are able to dominate *even the ensemble-averaged behavior* of the interference.

In Fig. 12, we compare the Fourier transform from one of the correlation functions and compare it with those calculated both classically and quantum mechanically for the 0.3-μm dot, in this case with a port opening of 0.06 μm. Figure 12(a) is the experiment, while Figs. 12(c) and 12(b) are those from the classical billiards and the quantum simulation, respectively. In all three cases, the spectra are quite similar and the resemblance between these curves is remarkable. The dominant peak in all cases is that near a magnetic frequency of 9 T^{-1}. As discussed above, this is closely correlated to the diamond wave-function plots. Thus the observed transport in the ballistic quantum dot is consistent with a model where the excitation of the dot is by a collimated beam, whether classically or quantum mechanically. To our knowledge, Fig. 12 provides the clearest evidence obtained to date for the direct manifestation of wave-function scarring in the transport properties of mesoscopic quantum dots.[2,4]

The implication of our results then is that in measurements of these *open* ballistic quantum dots, the trajectories that contribute to transport are *selected* by the nature of the input and exit ports. The overall transport properties are not necessarily descriptive of the complete spectrum of the dot, but are descriptive of those parts of the spectrum that are closely correlated to the selective properties of the ports. This same behavior has been seen in the wave function scarring in resonant tunneling diodes in tilted magnetic fields,[38] where only those orbits that couple effectively through the tunnel barrier are seen in the wave-function plots.[39] The behavior here, where a small family or families of *long* trajectories (long due to their apparent periodicity) is excited by the collimated beam and dominate the behavior, is quite different from that in a chaotic dot. In the chaotic case, *short* trajectories (an example being a trajectory going straight through from input to output ports) are believed to dominate due to a very dense distribution of eigenvalues.[31]

Before closing, we note that multiply periodic oscillations

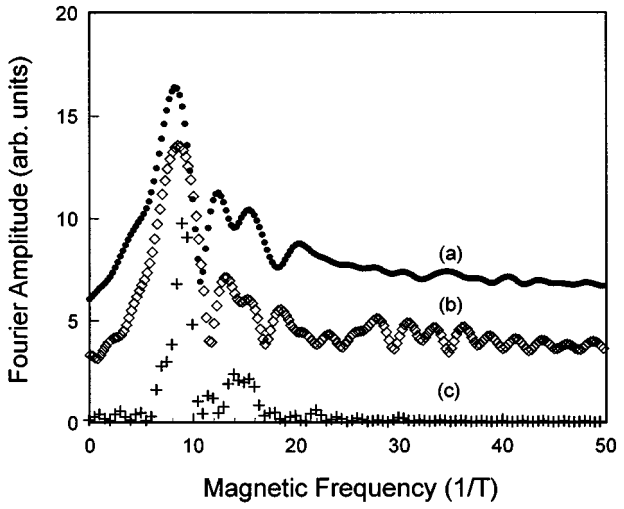

FIG. 12. Comparison of the spectra of the correlation functions for (a) the experimental dot, (b) the classical billiard, and (c) the quantum simulation for an effective dot size of 0.3 μm. The curves are offset for clarity.

in the transport of square quantum dots has been observed previously.[40,41] In contrast to the present work, this was with a four-lead geometry and the quantum Hall effect was the object of the study. In addition, the magnetic fields were much higher, so that edge states were present in the dot. In addition, the magnetic fields were much higher, so that edge states were present in the dot. The theoretical model[41] used to explain these results assumed that two of the edge states of the dot were involved in the transport, with one transmitted by the leads, the second forming a complete orbit trapped inside the dot. With mixing of the two edge states caused by the presence of leads, what resulted was a rather complicated version of the Aharoov-Bohm effect. While ''trapped'' orbits appear to be playing at least a superficially similar role in the results shown in the present case, we emphasize *strongly* that the orbits here are not of the ''skipping'' variety and cannot be associated with edge states.

V. CONCLUSION

In summary, we have presented studies of the quantum-mechanical transport and the classical billiard transport through ballistic semiconductor quantum dots. These were shown to have quite similar behavior, if the classical motion is limited to a collimated set of trajectories, presumably selected by the quantum-mechanical properties of the quantum point contacts by which leads are connected to the open quantum dots. These results are shown to agree substantially with experiments performed on actual semiconductor quantum dots, yielding highly oscillatory and correlated fluctuation spectra. This is fully in keeping with the expectations of semiclassical descriptions of the fluctuations in the density of states of such structures.

ACKNOWLEDGMENTS

The authors have benefited from helpful discussions with Richard Taylor, Anna Grincwajg, Barbara Sanborn, Andy Sachrajda, John Barker, Laurence Eaves, and Tom Szeredi. The work of R.A. and D.K.F. was supported in part by the Office of Naval Research and the Advances Research Projects Agency.

[1] See, e.g., P. A. Lee, A. D. Stone, and H. Fukuyama, Phys. Rev. B **35**, 1039 (1987).
[2] C. M. Marcus, A. J. Rimberg, R. M. Westervelt, P. F. Hopkins, and A. C. Gossard, Phys. Rev. Lett. **69**, 506 (1992).
[3] C. M. Marcus, R. M. Westervelt, P. F. Hopkins, and A. C. Gossard, CHAOS **3**, 643 (1993).
[4] A. M. Chang, H. U. Baranger, L. N. Pfeiffer, and K. W. West, Phys. Rev. Lett. **73**, 2111 (1994).
[5] R. P. Taylor, R. Newbury, R. B. Dunford, P. T. Coleridge, A. S. Sachrajda, and J. A. Adams, Phys. Rev. B **51**, 9801 (1995).
[6] I. H. Chan, R. M. Clarke, C. M. Marcus, K. Campman, and A. C. Gossard, Phys. Rev. Lett. **74**, 3876 (1995).
[7] J. P. Bird, K. Ishibashi, D. K. Ferry, Y. Ochiai, Y. Aoyagi, and T. Sugano, Phys. Rev. B **51**, 18 037 (1995).
[8] R. M. Clarke, I. H. Chan, C. M. Marcus, C. I. Duruöz, J. S. Harris, Jr., K. Campman, and A. C. Gossard, Phys. Rev. B **52**, 2656 (1995).
[9] J. P. Bird, K. Ishibashi, D. K. Ferry, Y. Ochiai, Y. Aoyagi, and T. Sugano, Phys. Rev. B **52**, 8295 (1995).
[10] M. Persson, J. Pettersson, B. von Sydow, P. E. Lindelof, A. Kristensen, and K. F. Berggren, Phys. Rev. B **52**, 8921 (1995).
[11] J. P. Bird, D. M. Olatona, R. Newbury, R. P. Taylor, K. Ishibashi, M. Stopa, Y. Aoyagi, T. Sugano, and Y. Ochiai, Phys. Rev. B **52**, 14 336 (1995).
[12] M. W. Keller, A. Mittal, J. W. Sleight, R. G. Wheeler, D. E. Prober, R. N. Sacks, and H. Shtrikmann, Phys. Rev. B **53**, R1693 (1996).
[13] See, e.g., *Gallium Arsenide Technology*, edited by D. K. Ferry (Sams, Indianapolis, 1995), Vol. I; *Gallium Arsenide Technology*, edited by D. K. Ferry (Sams, Indianapolis, 1989), Vol. II.
[14] A. Grincwajg, G. Edwards, and D. K. Ferry, Physica B (to be published); see also G. Casati and B. Chirikov, Physica D **86**, 220 (1995).
[15] R. A. Jalabert, H. U. Baranger, and A. D. Stone, Phys. Rev. Lett. **65**, 2442 (1990).
[16] H. U. Baranger, R. A. Jalabert, and A. D. Stone, Phys. Rev. Lett. **70**, 3876 (1990).
[17] W. A. Lin, J. B. Delos, and R. V. Jensen, CHAOS **3**, 655 (1993).
[18] H. U. Baranger, R. A. Jalabert, and A. D. Stone, CHAOS **3**, 665 (1993).
[19] See, e.g., K. Nakamura, *Quantum Chaos* (Cambridge University Press, Cambridge, 1993).
[20] Z.-L. Ji and K.-F. Berggren, Phys. Rev. B **52**, 1745 (1995).
[21] J. P. Bird, D. K. Ferry, R. A. Akis, Y. Ochiai, K. Ishibashi, Y. Aoyagi, and T. Sugano, Europhys. Lett. **35**, 529 (1996); J. P. Bird, D. K. Ferry, R. A. Akis, R. Newbury, R. P. Taylor, D. M. Olatona, Y. Ochiai, K. Ishibashi, Y. Aoyagi, and T. Sugano, Superlatt. Microstruct. **20**, 287 (1996).
[22] K. M. Connolly, D. P. Pivin, Jr., and D. K. Ferry, Superlatt. Microstruct. **20**, 308 (1996).
[23] C. W. J. Beenakker and H. van Houten, Phys. Rev. B **39**, 10 445 (1989); L. W. Molenkamp, A. A. M. Staring, C. W. J. Beenakker, R. Eppenga, C. E. Timmering, J. G. Williamson, C. J. P. M. Harmans, and C. T. Foxon, *ibid.* **41**, 1274 (1990).
[24] C. Jacoboni, P. Casarini, and A. Ruini, in *Quantum Transport in Ultrasmall Devices*, edited by D. K. Fery, H. L. Grubin, C. Jacoboni, and A.-P. Jauho (Plenum, New York, 1995), pp. 181–190.
[25] S. Fishman, B. Georgeot, and R. E. Prange, J. Phys. A **29**, 919 (1996).
[26] T. Usuki, M. Saito, M. Takatsu, R. A. Keihl, and N. Yokoyama, Phys. Rev. B **52**, 8244 (1995).
[27] T. Ando, Phys. Rev. B **44**, 8017 (1991).
[28] H. U. Baranger, D. P. Vincenzo, R. A. Jalabert, and A. D. Stone, Phys. B **44**, 10 637 (1991).
[29] E. J. Heller, Phys. Rev. Lett. **53**, 1515 (1984).
[30] M. C. Gutzwiller, J. Math. Phys. **12**, 343 (1971).
[31] R. Balian and C. Bloch, Ann. Phys. (N.Y.) **85**, 514 (1974).
[32] M. V. Berry and M. Tabor, Proc. R. Soc. London Ser. A **349**, 101 (1976); J. Phys. A **10**, 371 (1977).

[33] M. V. Berry, Proc. R. Soc. London, Ser. A **423**, 249 (1989).
[34] This has been examined for the ballistic dots of interest here by D. K. Ferry and G. Edwards (unpublished).
[35] While it is traditional to use action-angle coordinates for Poincaré plots, generally we find using the more basic position and momentum coordinates to be more intuitive in understanding the dynamics of the particles.
[36] R. Landauer, IBM J. Res. Dev. **1**, 223 (1957).
[37] M. Stopa, J. P. Bird, K. Ishibashi, Y. Aoyagi, and T. Sugano, Phys. Rev. Lett. **76**, 2145 (1996).
[38] T. M. Fromhold, P. B. Wilkinson, F. W. Sheard, L. Eaves, J. Miao, and G. Edwards, Phys. Rev. Lett. **75**, 1142 (1995).
[39] L. Eaves, T. M. Fromhold, F. W. Sheard, P. B. Wilkinson, N. Miura, and T. Takamasu, Physica B (to be published).
[40] C. J. B. Ford, S. Washburn, R. Newbury, C. M. Knoedler, and J. M. Hong, Phys. Rev. B **43**, 7339 (1991).
[41] G. Kirczenow and E. Castano, Phys. Rev. B **43**, 7343 (1991).